High mid-Holocene accumulation rates over West Antarctica inferred from a pervasive ice-penetrating radar reflector

Julien A. Bodart[1], Robert G. Bingham[1], Duncan A. Young[2], Joseph A. MacGregor[3], David W. Ashmore[4], Enrica Quartini[2,5], Andrew S. Hein[1], David G. Vaughan[6], and Donald D. Blankenship[2]

Supplementary Information

Assessing the suitability of the local-layer approximation

To quantify to what extent the assumptions used in the 1-D model are valid for estimating Holocene accumulation rates between the 4.72 ka IRH and the present, we calculated horizontal gradients in modern ice thickness and accumulation rates over the WAIS, and combined these to generate a non-dimensional parameter *D* spanning the catchments where the 4.72 ka IRH was traced (Waddington et al., 2007) (Fig. S1).

The input datasets used for this calculation were modern ice thickness from BedMachine v2 (Morlighem, 2020), modern Surface Mass Balance (1979 – 2019) from RACMO 2.3p2 (Van Wessem et al., 2018), and modern surface speed velocities (1996 – 2016) from the InSAR MEaSUREs v2 dataset (Rignot et al., 2017). These were all re-gridded to the same 1-km grid and smoothed using an exponentially decaying filter equivalent to ten ice thicknesses in length, before being decimated back to a common 5-km grid for data analysis. As per MacGregor et al. (2016), we re-calculated surface speed directions for slower ice-flow regions (<100 m a^{-1}) in the interior of the ice sheet using surface-elevation gradients from the BedMachine product. To calculate, L_{path} (Fig. S1a), we then produced a reverse flowline for each grid cell based on modern ice-surface speed, $\bar{u}$, and calculated where along the reverse flowline we obtained age, a, as follows:

$$L_{path} = \bar{u}\, a\,. \tag{S1}$$

We then interpolated the ice thickness and accumulation grids onto each flowline and conducted a first-order polynomial fit to obtain the ice thickness and accumulation gradients along the flowline. The ensuing gradients were then combined with the mean values along the flowline to calculate the characteristic lengths L_H and $L_{\dot{b}}$ (Fig. S1b-c), as follows:

$$\frac{1}{L_H} = \left|\frac{1}{H}\frac{dH}{dx}\right|. \tag{S2}$$

$$\frac{1}{L_{\dot{b}}} = \left|\frac{1}{\dot{b}}\frac{d\dot{b}}{dx}\right|. \tag{S3}$$

Taken together, the ice thickness and accumulation gradients were combined to obtain a characteristic length scale, which was used to compare with L_{path} to generate the non-dimensional parameter *D* (Fig. S1d):

$$D = L_{path}\left(\frac{1}{L_H} + \frac{1}{L_{\dot{b}}}\right). \tag{S4}$$

Values where $D < 1$ indicate that local horizontal gradients in ice thickness and accumulation rates have a smaller effect on IRH depth of age a, and hence we assume that the LLA is valid for estimating accumulation rates for an IRH of age a (Waddington et al., 2007; MacGregor et al., 2009) (Sect. 2.2.1).

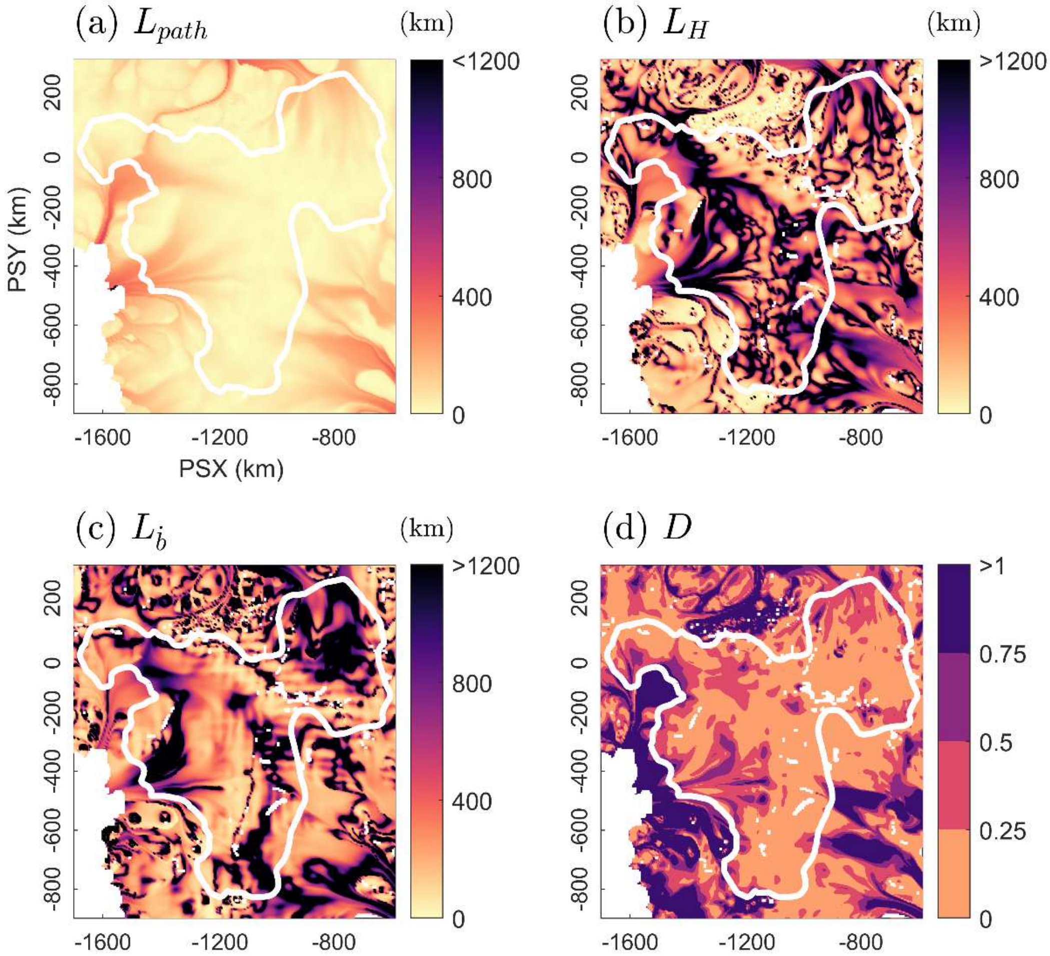

Figure S1. Suitability of the Local-Layer Approximation over the Pine Island, Thwaites, and Institute and Möller ice-stream catchments for the 4.72 ka IRH. (a) Horizontal path length of a 4.72 ka particle of ice to reach its present location, calculated using modern surface speeds (Rignot et al., 2017). (b) Characteristic length of ice thickness variability along the 4.72 ka particle path, estimated using modern ice thickness measurements from BedMachine v2 (Morlighem, 2020). (c) Characteristic length of accumulation variability along the 4.72 ka particle path, estimated using modern modelled SMB data from RACMO2 (Van Wessem et al., 2018). (d) The D parameter for the 4.72 ka IRH used to quantify the suitability of the LLA for the survey area. The white outline represents the model domain boundary used to model Holocene accumulation rates where $D = 1$.

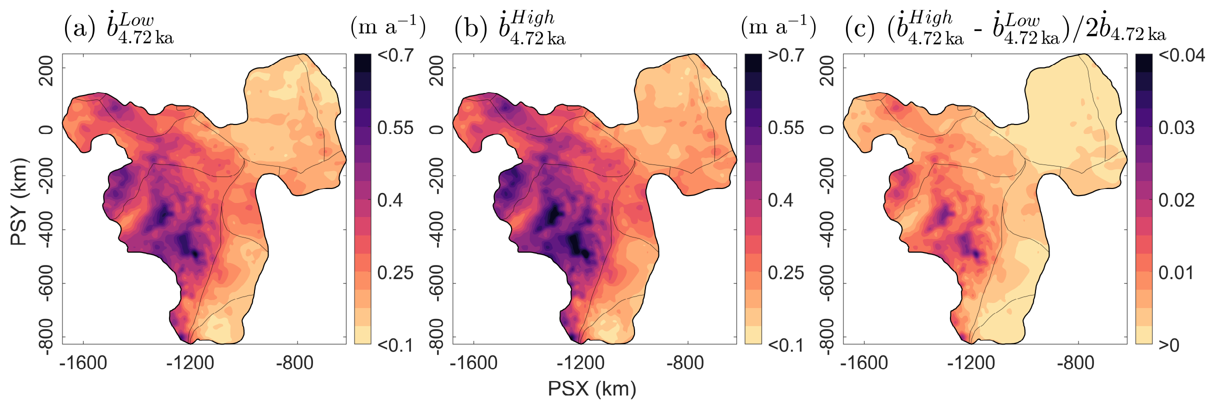

Figure S2. Uncertainty in accumulation rates based on the radar and ice-core age uncertainties. (a) Lower bound accumulation estimates from the lowest possible age of the 4.72 ± 0.28 ka IRH based on radar and ice-core uncertainties in age (Muldoon et al., 2018; Bodart et al., 2021). (b) Upper bound accumulation estimates from the highest possible age of the 4.72 ± 0.28 ka IRH based on radar and ice-core uncertainties in age. (c) Relative uncertainty in accumulation rates for the 4.72 ka IRH based on the equal lower and upper bound (± 0.28 ka) estimates, following MacGregor et al. (2016).

Following MacGregor et al. (2013), we calculated longitudinal strain rates, σ, from gradients in the x and y-direction for modern surface speeds ($\bar{u}$) projected onto the appropriate surface velocity unit vectors ($\hat{u}_{||}$), as follows:

$$\sigma = \frac{\partial u}{\partial x} = \overline{\nabla}|\bar{u}| \cdot \hat{u}_{||}. \tag{S5}$$

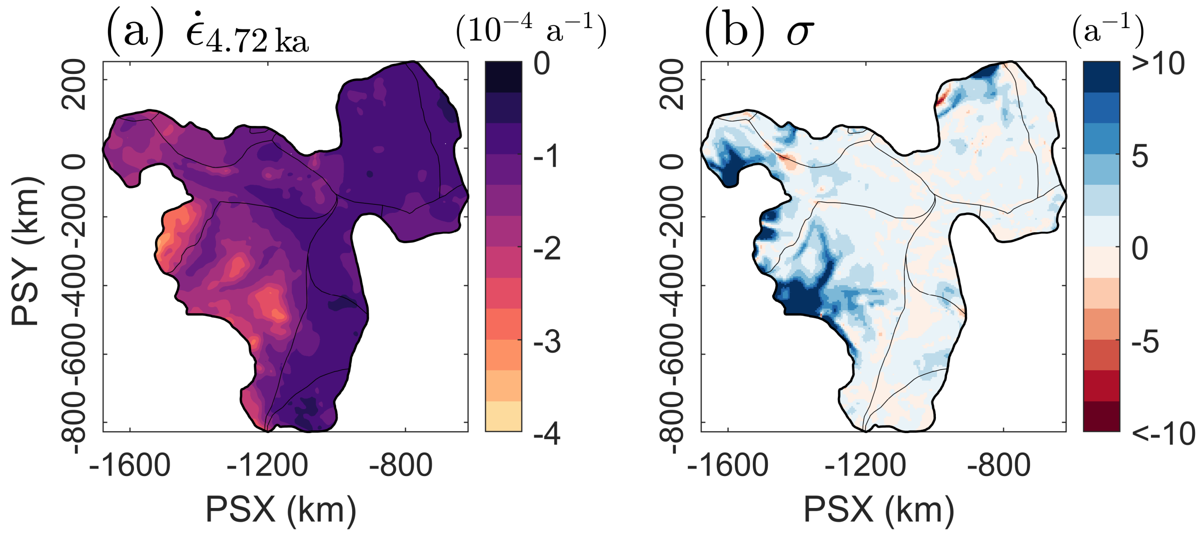

Figure S3. Strain rate patterns over the survey area. (a) Mean vertical strain rates, $\dot{\varepsilon_a}$, for the 0-4.72 ka portion of the ice column calculated from Eq. (2) (b) Longitudinal strain rates, σ, obtained from Eq. (S5).

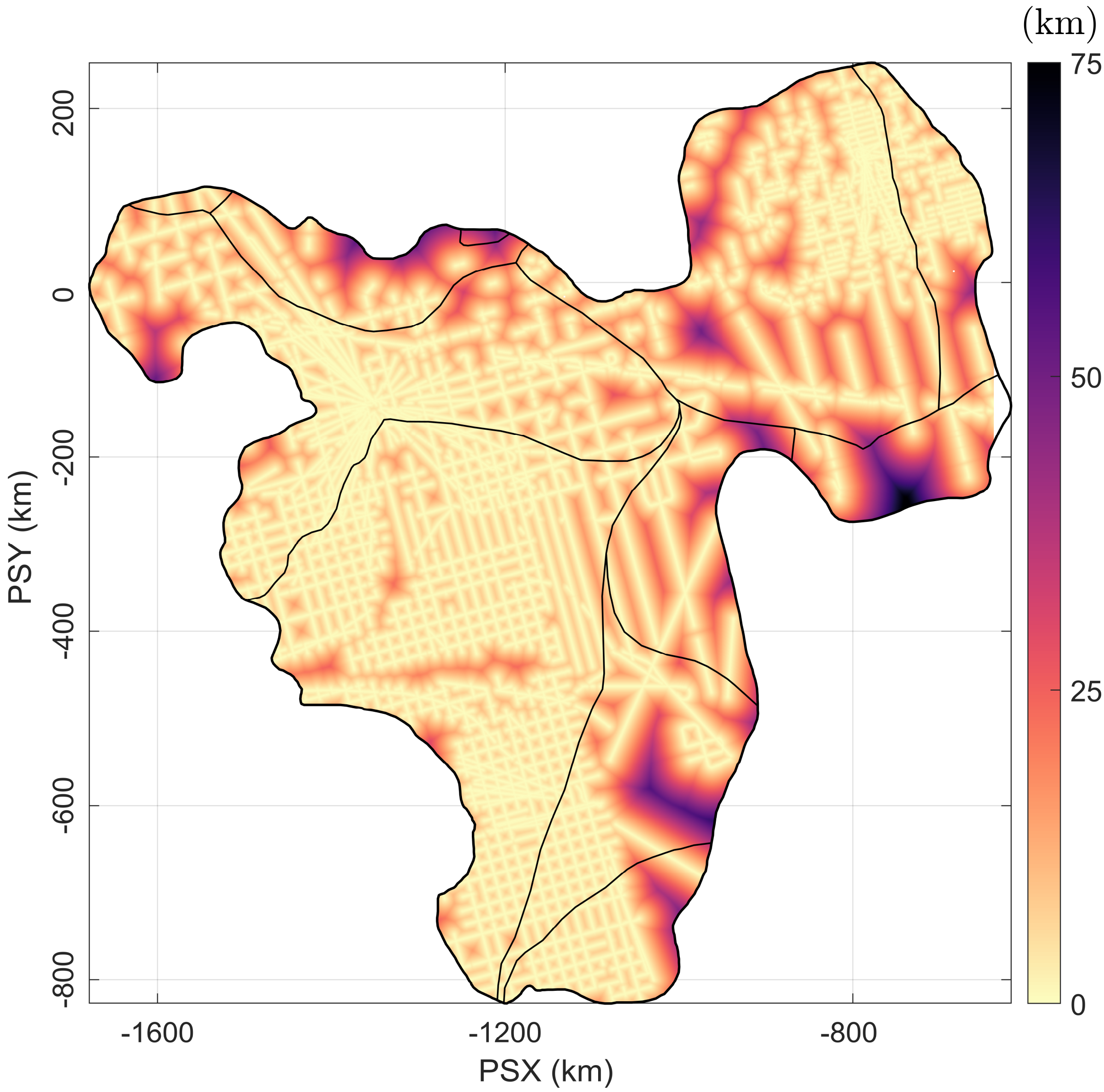

Figure S4. Maximum distance to the nearest 500-m along-track point used for the interpolation of the 4.72 ka IRH depth and accumulation grids.